**Stable coexistence and transport of lytic phage infections with migrating bacterial hosts**

Jacopo Marchi[1,*], Chadiga Khalek[2,3,4,*], Abir George[5], Joshua S. Weitz[1,6,7,^], Remy Chait[2,3,4,^]

[1]Department of Biology, University of Maryland, College Park, MD, 20742, USA

[2]Biosciences, University of Exeter, Exeter, EX4 4PY, UK

[3]Living Systems Institute, University of Exeter, Exeter, EX4 4QD, UK

[4]Natural Sciences, University of Exeter, Exeter, EX4 4PY, UK

[5]Lewis-Sigler Institute for Integrative Genomics, Princeton University, Princeton, New Jersey 08540, USA

[6]Department of Physics, University of Maryland, College Park, MD, 20742, USA

[7]University of Maryland Institute for Health Computing, North Bethesda, MD, 20852, USA

* Authors contributed equally to this work.

^ Correspondence: RC (r.chait@exeter.ac.uk) & JSW (jsweitz@umd.edu)

## Abstract

Bacteriophages (phages), viruses that exclusively infect bacterial hosts, are the most abundant living entities across diverse environments, coexisting with their bacterial hosts at densities exceeding $10^7$ $ml^{-1}$ in marine surface waters, $10^8$ $ml^{-1}$ in soils, and $10^9$ $ml^{-1}$ in the human gut[1–6]. In contrast, virulent phage rapidly lyse bacteria populations within well-mixed *in vitro* environments, selecting for the emergence of phage-resistant bacterial mutants[7], which in turn select for host-range expansion phage mutants[8], leading to the emergence of complex cross-infection networks[9], and eventually the collapse of phage populations altogether[10,11]. This gap in outcome raises a question: what enables long-term phage-bacteria coexistence? Here, we show how interactions in space can facilitate stable coexistence and long-range transport of virulent phage along with migrating bacteria. Through the joint use of theory, simulation, and experiments across multiple phage-bacteria systems, we reveal a chemotaxis-driven mechanism which robustly stabilizes coexistence and dispersal of virulent phages with migrating hosts, while minimizing the potential for coevolutionary-induced collapse of either bacteria or phage. These findings suggest the ecological relevance of spatial interaction mechanisms that reinforce stability between antagonistic partners, even in the absence of perpetual cycles of defense and counter-defense, that may be broadly applicable across phage-bacteria pairs.

## Introduction

Phage infection can lead to the rapid takeover of cellular machinery, phage genome replication, self-assembly of capsids, cellular lysis, and the release of dozens if not hundreds of infectious virions[12–15]. The death of individual cells does not necessarily eliminate entire bacterial populations due to the self-limiting nature of infections[16,17]. In the near-term, obligately lytic phage and their bacterial hosts can coexist given predator-prey like dynamics with phase-shifted peaks in phage and bacterial abundance as predicted via nonlinear dynamic theory[18] and validated in chemostats[19–21]. On longer time scales, strong pressure to resist phage-induced lysis by bacteria and corresponding pressure to infect mutant bacteria by phage can drive complex eco-evolutionary dynamics.

Instead of perpetual, phase-shifted population dynamics, the process of bacterial resistance and phage counter-resistance can lead to increased resistance of evolved bacteria to current and prior phage strains and expanded host range of evolved phage with respect to current and prior bacterial strains[10,22,23]. The resulting 'nested' interaction structures observed across diverse environments reflect the potential for long-term phage-bacteria coexistence mediated by coevolutionary arms race

dynamic[9,24,25] – even as more complex dynamics reflecting a mix between arms races and specialization can unfold jointly within multiscale phage-bacteria modules both in natural systems[26,27] and in *in vitro* experiments[11]. However, despite these mechanisms, the coevolutionary process in laboratory settings typically leads to the emergence of phage-resistant bacterial mutants that phage cannot infect even after multiple rounds of coevolution[10,11,28], consistent with a hypothesized 'asymmetric advantage'[8] in bacterial evolutionary potential relative to phage.

In contrast to well-mixed laboratory conditions, population dynamics and community structure of complex microbiomes are shaped in part by spatially explicit interactions[29–32]. Spatially-localized systems can exhibit markedly different behaviour than their well-mixed counterparts – including the potential for sustained diversification and coexistence amongst parasites and hosts[30,32–37]. Spatial structure can also reshape the potential for phage-bacteria coexistence. Motile bacteria may be able to migrate orders of magnitude faster over ecologically relevant timescale than is possible through phage diffusion alone. While phage can infect and proliferate quickly, bacteria that move beyond zones of infection can escape infections entirely. The potential for motility-enabled escape from parasitism is analogous to theories underlying long-distance seed dispersal in plants[38,39] and raises questions on whether spatial interactions enhance or suppress phage-bacteria coexistence.

Previous experimental and modelling efforts have measured interactions between chemotactically migrating bacteria and obligately lytic phage[40–42]. These studies have shown that active phage infections can co-propagate with bacterial hosts over short length scales on the order of cm-s, but that long range co-propagation may require fine tuning of phage and host parameters[42] and is sensitive to phage resistance of hosts arising during transient dynamics[40]. To address the impact of spatial interactions on the coexistence of virulent phage with motile bacteria, we used large format timelapse imaging of agar swim assays to explore the emergent dynamics of migrating bacterial hosts that encounter virulent phage in spatially explicit contexts over longer spatial and temporal scales. In doing so we discovered that virulent phage can propagate with migrating bacterial fronts stably over the equivalent of dozens if not hundreds of bacterial generations at speeds an order of magnitude faster than when spreading through static bacterial lawns. Through a combination of theory, models, and experiments, we identify principles underlying the emergence of stable transport of infections in diverse phage-bacteria systems and consequences for phage-bacteria coexistence more broadly.

**Lytic phage invasion and propagation with migrating bacterial fronts**

We initiated spatial infection experiments by inoculating a localized 1µl drop of virulent phage lysate approximately 2 cm away from a localized 1µl drop of phage-sensitive, chemotactic bacterial culture in large format, soft agar swim plates. By inoculating the bacterial host near the corners of 12cm and 24cm square culture plates and collecting high-resolution timelapse images of the expanding bacterial population and lytic clearing zones with a scanner-based platform (see Methods), we were able to follow propagating host-phage dynamics for days over distances up to 25cm . Figure 1a shows the results of inoculating an LB swim plate containing 0.25% agar with virulent *Escherichia phage* T7 and *E.coli* K12 strain W1485(F8) pre-adapted to swim assays to reduce the emergence of "fast" mutants[43] (for all strains see Methods). Phage T7 had a dramatic effect on encounter by the migrating bacterial front, rapidly lysing hosts and inducing the emergence of a widening front invasion clearance zone. This clearance zone was then protected from immediate bacterial re-invasion (Figure 1A, 14-21h, Supplementary Movie 1, and Supplementary Figure 1). Despite the dramatic lysis-induced disruption of the expanding bacterial front, the chemotactic bacterial population continued to propagate outward without interruption in regions outside the clearance zone, slightly outpacing the infection and curving gradually inwards (Figure 1A, 21h-27h). As the two propagating bacterial fronts on either side moved inward, the phage cleared zone grew narrower and the inward curvature ceased (Figure 1A, 31h). However, rather than being trapped behind the merged front once the two fronts converged, the phage infection coalesced to a focused clearance zone and then propagated stably with the bacterial front at a speed of ~5mm/hr (Figure 1A, 31h-48h). Notably, the velocity of the migrating bacterial front transporting the phage infection is an order of magnitude greater than conventionally measured velocities of 0.2-0.25 mm/hr for T7 plaque expansion in static, bacterial populations[44].

We repeated the experiment with *E. coli* K12 strain W1485(F9), a mutant of W1485(F8) with a single, dominant chemotactic front which migrates approximately 40% faster (~7.2mm/hr). Encounter of phage T7 by this faster single-front *E. coli* mutant leads to qualitatively similar dynamics, including a front invasion transient clearance zone, inward curvature of bacterial fronts on either side of the clearance zone, and finally coalescence to a stably propagating infection and phage-cleared zone in the center of the migrating bacterial front (Figure 1C). Stable infection transport also emerged across other phage and host bacteria combinations we tested, *e.g.*, phage T4 and *E.coli* W1485(F8) (Figure 1D) and phage phiKZ and *P. aeruginosa* PA01 (Figure 1E). In each case we observed the stable propagation of narrow phage-induced clearance zones originating at the leading edge of the migrating bacterial front (see blue highlighted panels in Figure 1B-E). We refer to the propagating phage infection and associated cleared zone within bacterial chemotactic fronts as a Phage-Amplified Spatially Extended Region or "PhASER". The stable establishment and persistence of PhASERs across multiple phage-bacteria systems with distinct bacterial chemotactic mechanisms and phage life history traits suggests the relevance of common, eco-physical principles.

**Stabilization of phage transport along population-mediated chemical gradients**

To explore the basis for PhASER emergence, we developed a nonlinear, partial differential equation (PDE) model of the spatiotemporal dynamics of phage-sensitive and infected bacteria, virulent phage, resources, and chemoattractant molecules (see Box 1). The model combines principles of chemotactic range expansion in bacteria[43] with infection-mediated feedback mechanisms used in ecological models of phage and bacteria[17,40,44]. In this reaction-diffusion-advection model, bacteria take up resources, reproduce, and migrate up gradients generated by chemoattractant depletion while phage adsorb to and infect bacteria that themselves continue to migrate, eventually lysing and releasing infectious virions back into the soft agar environment (see Box 1 for a schematic and overview of model ingredients and Supplementary Text for a complete description of model equations and parameters, including the use of a discreteness threshold for phage reaction terms). The underlying reaction-diffusion-advection model includes key feedback terms: (i) phage lysis inhibition in resource-depleted environments[45,46]; (ii) explicit accounting for infected stages corresponding to non-exponential latent period distributions[44,47]. Removal of either destabilizes spatiotemporal dynamics (see Supplementary Figure 2).

The resulting reaction-diffusion-advection model generates stable phage invasion and transport patterns at population scales that are both qualitatively and quantitatively consistent with PhASERs observed in large-format agar plate experiments. Figure 2 shows model-simulated dynamics of phage infection and long-range transport using parameters estimated for E.coli W1485(F9) and phages T7 and T4 (see Supplementary Text) alongside experimentally measured data for the same strains (Supplementary Movies 2-5). In both cases, the model exhibits an initial expansion of a lytic clearance zone, coalescence to a focused infection in the chemotactic front, and the stable migration of this phage infection at the same speed as the migrating bacterial population (simulations for phage T7 and T4 lead to PhASERs propagating on host bacterial fronts migrating at 7.2 mm/hr and 6 mm/hr, respectively, consistent with corresponding experiments). Curved lines overlaid over late-stage images (Methods, Supplementary Figure 3) show the correspondence of experimental and simulated migrating bacterial front positions at 2-hr intervals (independent of phage lysis of static lawn behind fronts). Model simulations also exhibit qualitatively similar front invasion transients with wider phage T7 than T4 clearance zones before coalescence to a stable PhASER, and more rapid erosion of the static host lawn behind the fronts by phage T7.

**Box 1: Reaction-diffusion-advection model of phage infections of chemotactic bacteria**

Summary: We developed a nonlinear system of partial differential equations (PDEs) governing the reaction-diffusion-advection dynamics of chemotaxing susceptible ($S$) and infected ($E$) bacteria, phage $P$, resources $R$ (magenta gradient) and chemoattractant $a$ (green gradient). All population types diffuse according to a corresponding type-specific diffusion constant $D$. For bacteria, the diffusion represents the random component of a run-and-tumble process[48] rather than Brownian motion. For viruses, resources, and chemoattractants, the diffusion represents that expected via Brownian motion.

Reaction terms – bacterial uptake and growth: All bacteria consume resources represented in cell density units (CFU/mL) and only susceptible cells divide given a resource-dependent function $g(R) = \frac{rR}{R+K}$, where $r$ is the maximum growth rate and $K$is the Monod constant. We assume that infected cells do not divide. Chemoattractant molecules are consumed according to a chemical-specific Monod law with rate $\mu(a_n) = \frac{\mu_{n,\max} a_n}{a_n + K_n}$.

Reaction terms – phage infection, lysis, and decay: Phage adsorb to all bacteria and initiate infections in susceptible bacteria given a functional form *F(P)* that varies with phage. For T7, $F(P) = \phi P$ with adsorption rate $\phi$ while for T4, we use a nonlinear profile $F(P) = \phi \frac{P}{1+P/P_c}$ with a saturating phage density $P_c$. Phage saturation mimics Michaelis-Menten reaction kinetics mediating competition by coinfecting phage[49]. Infected cells progress through $L$ infection stages $E_{i\in\{1\ldots L\}}$ before lysis – these stages are a mathematical convention to represent latent periods as an Erlang distribution[44] with an average latent period $1/\eta(R)$ and variance controlled by $L$. Lysis produces $\beta(R)$ virions. We assume that the lysis rate $\eta(R) = \eta \frac{R}{R+K}$ and burst size $\beta(R) = 1 + \beta \frac{R}{R+K}$ depend on growth rate such that phage lysis halts in the absence of available resources and lysis (when it occurs) has a minimum burst size of 1. Finally, phage decay at a rate $\omega$ per virion. Note that all phage reaction terms, are modulated by a nonlinear function $T(P) = \frac{P^M}{P^M + \Theta^M}$, where $\Theta$ is a discreteness threshold scaling as the inverse of the volume of the PDE integration lattice sites (see Supplementary Text for numerical implementation) with large Hill coefficient $M$. This nonlinearity scales from 0 for $P \ll \Theta$ to 1 when $P \gg \Theta$ and ensures that phage, the fastest dynamical variable in the system, do not diffuse and subsequently infect cells far from the inoculation point before they reach biologically realistic densities (see Supplementary Text).

Advection terms – chemotaxis: Bacteria sense attractant gradients and chemotax towards higher concentrations given the self-generated velocity field $v(a_n) = \chi \nabla \ln\left(\frac{1+a_n/a_-}{1+a_n/a_+}\right)$, which triggers a collective population range expansion wave[43,50]. The sensing function takes a logarithmic Weber form[43,51] with two sensitivity parameters $a_-$ and $a_+$ respectively denoting the lowest and the highest chemoattractant densities bacteria react to. For simplicity, we assume that the velocity field function does not depend on the attractant type $n$ through the parameters $a_-$, $a_+$ and $\chi$ denoting bacteria responsiveness to sensed chemical gradients. Infected cells also sense differences and chemotax towards higher concentrations with a potentially different efficiency than uninfected cells.

**Attractant-mitigated infection-chemotaxis feedback drives dynamical Robustness of PhASERs**

We leverage PDE model simulations to explore feedback mechanisms responsible for PhASER emergence, persistence, and stability. Figure 3A shows timepoints from a simulation where bacteria, sensing a single attractant, give rise to a single range expansion front[43]. When the front encounters and is invaded by phage, a lysis region spreads out before the fronts regions on either side slowly curl back inwards and converge, just like in the experiments shown in Figure 1. The first inset in the second row of Figure 3A shows that this convergence is driven by an infection-induced curvature in the attractant gradient (green isolines) that arises from reduced consumption due to phage killing of host cells in the center. The bacteria migrate orthogonally across the isolines in the direction of the chemotactic flux (see arrows in Figure 3A). At the same time, infected cells (blue colormap), which migrate together with non-infected ones, lyse and release new free phage (red colormap in Figure 3A) close to the front. Susceptible cells moving inward interact with free phage and transport them during infection as shown by the change in color of the flux arrows, denoting the fraction of infected cells. Once the two wings of infection transport reunite, they influence one another's chemotactic collective behavior through the chemoattractant profile, which merges the attractant isoline, forming a cusp (second inset in Figure 3A, second row). As a result, the cells at the merging point exhibit a high infection prevalence and accumulate along the symmetry line. The lagging, cusp-shaped front produces a steeper chemical gradient and therefore a higher flux in the center of the front-associated

clearance zone (Figure 3A, third inset). This higher flux relative to adjacent regions allows infected cells to migrate forward faster ensuring the dynamical stability of PhASER propagation.

After some time, the dynamics stabilize to a steady state where the infection transport remains unaltered as the wave progresses, as indicated by the conserved flux profiles across the front in the fourth inset of Figure 3A. The infection is focused by the convergent migration of cells up the nutrient gradient toward the symmetry line. Infected cells then migrate with the expansion front, eventually lysing and producing free phage which in turn infect new cells in the front ensuring a long-range stable infection transport. The control of bacterial densities due to lysis maintains slower chemoattractant consumption in the infected front region. This slower consumption changes the curvature of the gradient such that the fronts of uninfected cells bend inwards, producing the observed front curve ensuring a steady influx of susceptible cells into the front region where phage infection is active. This convergent migration towards the symmetry line also focuses the infection and constrains its lateral spread. We stress that such range expansion is a population-driven collective behavior akin to chemotaxis of bacteria in the absence of phage[49]. Therefore should a few cells (infected or not) move ahead of the front due to random fluctuations in their chemotactic process these cells will not generate a sufficient attractant gradient to sustain range expansion and the fluctuation will dissipate[52]. Finally, chemotaxis into the nutrient-rich zone cleared by the invading phage slows its outward expansion which terminates early due to resource limitation.

The processes of PhASER emergence, persistence and stability apply to model simulations using the same parameters inferred on dynamics of T7 with *E. coli* W1485(F8) strain (see Supplementary Text), albeit with inclusion of a second chemoattractant molecule, which produces a second chemotactically migrating front, similar to that observed for W1485(F8) and its W1485 ancestor in LB swim agar (Figure 3C). Finally, we modified the phage life-history traits in model simulations to correspond to phage T4 (including the infection rate, maximum lysis rate, and burst size) while keeping the bacteria parameters fixed. Model simulations can qualitatively recapitulate experimentally observed T4 dynamics (see Figure 3C), generalizing our finding for model simulations with a single front (as shown in Figure 2).

**PhASER initiation is robust to infection-reduced chemotaxis**

Bacteria maintain a diversity of anti-phage defense systems and physiological responses to phage infection[50–52]. In the case of a spatially explicit infection, we hypothesized that any mechanism that reduced chemotaxis efficiency within infected cells would eventually lead to PhASER termination. We chose to evaluate a generalized mechanism: whether migrating cells could escape stabilization of the transient clearance zone to a propagating PhASER through a reduction in chemotactic efficiency of infected cells. Such a reduction in efficiency could arise because infected cells achieve a weaker chemotactic bias up attractant gradients. We hypothesized that there would be a critical threshold below which reduction in the chemotactic efficiency of infected cells would lead to PhASER termination. We tested this hypothesis in the reaction-diffusion-advection model by assuming that infected cells perform chemotaxis with responsiveness $\tilde{\chi} = \alpha\chi$ with $\alpha$ between 0 and 1 relative to uninfected cells. Note that in our formalism this parametrization is also equivalent to a scenario where at any point in time a fraction $\alpha$ of the infected cells chemotax. As expected, when infected cells have low chemotactic efficiency, the infection is lost behind the range expansion front. Surprisingly, the system was remarkably tolerant to reduction of infected cells chemotaxis – we found PhASER maintenance and infection transport was only lost below a chemotactic responsiveness threshold between 70% and 75% that of uninfected cells (Figure 3D). Note that the threshold for infection transport depends on the phage infection parameters. For example, phage T4-parameterized PhASERs maintain the ability to propagate only as long as chemosensing responsiveness exceeds 85% to 87% relative to uninfected cells (see Supplementary Figure 4). This finding reinforces the central role of infected cell migration in the generation, stability, and persistence of PhASERs.

**PhASERs are robust to large-scale environmental perturbations**

We set out to assess the robustness of PhASERs to large-scale environmental perturbations. First we modulated the agar density, which impacts the movement of cells in swim plates, slowing the progress

of chemotaxing bacteria with increasing agar concentration. We found that stable infection transport was robust to a wide range of agar concentrations, corresponding to dramatic differences in range expansion speeds from 3.5 to 8.5 mm/hr (Fig 4A). The model reproduces this robustness, as we could adapt the chemosensing responsiveness $\chi$ and the bacteria diffusion constant $D_B$ to reproduce the PhASERs patterns at the experimentally measured range expansion speeds. We note that when the agar concentration is sufficiently high it can disrupt regular chemotactic range expansion which in turn leads to the failure of stable infection propagation (Supplementary Figure 5).

Second, we explored the impact of mutant propagation speed on PhASERs. We do so because in migrating bacterial systems there is a particularly strong selection for mutants with enhanced front propagation speeds[49]. Here, we asked whether naturally occurring migration speed mutants of our ancestor bacterial strain would potentially disrupt PhASER formation and stability. We observe that as in the case of the faster expanding W1485(F9), a mutant W1485(F10) that gives rise to much faster range expansion than its parent W1485(F8) but with two chemotactic fronts, nonetheless reliably produces PhASERs both in simulations and in experiments (Fig 4B). This finding agrees with the observation that mutations affecting the number of range expansion fronts (i.e., single or double) does not noticeably impact PhASER emergence, propagation, and stability (Fig. 2).

Finally, we examined how the size of the phage inoculum impacted its invasion of the migrating bacterial front and the emergence of stable, long-distance infection transport. To do so, we challenged migrating bacterial fronts with phage inoculi containing either phage T4 or T7 at numbers of plaque forming units (PFUs) spanning several orders of magnitude . Strikingly, we observed that just a few PFUs of T7 reliably invade the host front and initiate PhASERs (see experiments and model in Figure 4C). In contrast, the less virulent phage T4 produced increasingly extended plaques with larger inoculi but was unsuccessful in invading the migrating front and initiating stable infection transport below a threshold level between $10^3$ and $10^4$ PFUs. We posit that this migration-mediated Allee effect[53] is driven by a requirement for a sufficient initial deformation of the chemotactic front to enable convergence of cells into an infection region and establishment of a stable proliferating phage population, instead of their gradual dilution and loss as the perturbed migrating front advances. This geometric perturbation is only attained by sufficient killing at high T4 phage concentrations, which triggers a positive feedback wherein the phage-invaded front slows down due to slower chemical consumption, generating a sustained influx of susceptible cells for infection to establish the stable PhASER. Our model reproduces this qualitative trend showing the absence of an Allee effect for T7 parameters and the presence of an Allee effect for T4 parameters, (albeit, at a different inoculum range than experiments), when T4 infected cells have slightly reduced chemotactic efficiency (Fig 4C).

**Dynamical robustness of interactions between PhASERs and with other migrating populations**

In order to probe the infection transport stability of PhASERs in complex, dynamic contexts we set out to investigate collisions between PhASERs and of PhASERs with non-infected migrating bacterial waves. By inoculating cells and phage at multiple locations on the agar swim plates, we were able to initialise and specify the direction of multiple PhASERs translocating on the same plate. We first grew two colonies from different locations, each transporting a PhASER, towards a common location. When equivalently translocating PhASERs collide at a shallow (60 degree) angle, they merge in their average direction (Fig. 5A). Numerical simulations of our model reproduce this phenomenon, and reveal that this dynamic stability is enabled by precisely the same feedback that permits stable coalescence of the two sides of the invasion transient that produces T7 PhASERs. Simulations reveal that as the two outer fronts of the PhASERs merge, the infected cells along the symmetry line are propelled faster into the uncolonized region by the attractant gradient cusp and by the presence of more cells at the colonies merging interface (Fig. 5B, Supplementary Movie 6). In contrast, when we repeated the experiments with two PhASERs merging at a much steeper (120 degree) angle, the collision resulted in a termination of the transport process both in the experiments and in the model (Fig. 5C). The simulations revealed that when the relative angle of two approaching fronts is too steep, the radial portion carrying phage is lost in the bulk behind the resulting front, as the phage-free sectors of the expanding populations merge and close the nutrient-rich corridor faster than the infections can travel to keep up with the front (Fig. 5D, Supplementary Movie 7). Similar outcomes

are obtained when PhASERs collide with walls in the environment at different angles (Supplementary Figure 6). Together, these results reinforce the importance of geometry underlying robust ecological dynamics[53]. Finally, we tested the stability of infection transport to complex ecological interactions featuring competition between different host traits. We merged a colony of F8 strain carrying a T4 phage PhASER with a significantly faster colony of strain F10 (experimental front speeds of 4.5 mm/hr vs. 6.5 mm/hr, respectively). We found that despite the mismatched hosts, the propagating phage infection transfers to the faster strain, turning sharply and continuing to stably propagate on the curved interface where the two populations merge (Fig 5E, Supplementary Movie 8). This behaviour is closely reproduced by the model without needing to adjust any parameters, underscoring the generality of predictions within our reaction-diffusion advection framework (Fig 5E, Supplementary Movie 9), including robustness to differences in phenomenological representations of phage adsorption (Supplementary Figure 7).

**Conclusions**

Our experiments reveal how stable coexistence and long-range transport of infections spontaneously emerge from interactions between virulent phage and migrating bacterial hosts. We developed and analyzed a mathematical model combining phage infections and chemotactic bacterial migration, unveiling a key feedback in which local phage killing reduces nutrient consumption, establishing a concave nutrient gradient that draws in susceptible hosts and projects infected cells to an infection tip in a migrating bacterial front. The emergence and stability of phage infection transport over long distances is enabled by transport of infected cells and applies to a diversity of phage-bacteria systems. Combining theory and experiments, we characterized the emergence of a robust balance between infection propagation and chemotactic escape in spatial environments, enabling long range rapid transport of bacteriophages and stable coexistence even in the absence of coevolutionary arms races. We envision that this study will help pave a path towards integrating eco-physical and eco-evolutionary mechanisms underlying phage-bacteria coexistence in complex habitats.

**Data Availability**

The datasets generated and/or analysed during the current study are available as image and movie files as shown in the Main Text and in the Supplementary Information.

**Acknowledgements**

We are grateful to B. Temperton, T. Bergmiller, N. Nikolic, W. Moebius, E.S. Tamar, R. Kishony, I. Golding, S. Pagliara, A. Andersson, N. Stitt, M. Cooper, I. Parry, and the members of Exeter's Bacterial Pathogenicity Research Group and University of Maryland's Quantitative Viral Dynamics Group for helpful discussions and suggestions. We thank N. Nikolic, C. Fitch, B. Temperton, S. Porter, S. van Houte, R. Sorek, W. Moebius for kind gifts of strains and Exeter's Physics Machine Shop and Microfluidics Facility for technical assistance. The research leading to these results was made possible via funding from Exeter Biosciences (RC), EPSRC Summer Internship (CK), Exeter Access2Internship (CK), Simons Foundation 930382 (JSW) and support from the Chair Blaise Pascal program of the Île-de-France region (JSW, JM, and AG).

**References**


1. Wigington, C. H. *et al.* Re-examination of the relationship between marine virus and microbial cell abundances. *Nature Microbiology* **1**, 15024 (2016).
2. Rohwer, F. & Thurber, R. V. Viruses manipulate the marine environment. *Nature* **459**, 207–212 (2009).
3. Roux, S. *et al.* Ecogenomics and potential biogeochemical impacts of globally abundant ocean viruses. *Nature* **537**, 689–693 (2016).
4. Edwards, R. A. *et al.* Global phylogeography and ancient evolution of the widespread human gut virus crAssphage. *Nat Microbiol* **4**, 1727–1736 (2019).
5. Manrique, P. *et al.* Healthy human gut phageome. *Proc. Natl. Acad. Sci. U.S.A.* **113**, 10400–10405 (2016).
6. Chevallereau, A., Pons, B. J., van Houte, S. & Westra, E. R. Interactions between bacterial and phage communities in natural environments. *Nature Reviews Microbiology* **20**, 49–62 (2022).
7. Luria, S. E. & Delbrück, M. Mutations of Bacteria from Virus Sensitivity to Virus Resistance. *Genetics* **28**, 491–511 (1943).
8. Lenski, R. E. Coevolution of bacteria and phage: are there endless cycles of bacterial defenses and phage counterdefenses? *Journal of Theoretical Biology* **108**, 319–25 (1984).
9. Flores, C. O., Meyer, J. R., Valverde, S., Farr, L. & Weitz, J. S. Statistical structure of host–phage interactions. *Proceedings of the National Academy of Sciences* **108**, E288–E297 (2011).
10. Meyer, J. R. *et al.* Repeatability and contingency in the evolution of a key innovation in phage lambda. *Science* **335**, 428–432 (2012).
11. Borin, J. M. *et al.* Rapid bacteria-phage coevolution drives the emergence of multi-scale networks. *Science* **382**, 674–678 (2023).
12. Abedon, S. T. Bacteriophage ecology: population growth, evolution and impact of bacterial viruses. in (ed. Press, C. U.) doi:10.1017/CBO9780511541483 (Cambridge University Press, Cambridge, UK).

13. Delbruck, M. The growth of bacteriophage and lysis of the host. *J. Gen. Physiol.* vol. 23 643–660 (1940).
14. Judson, H. B. *The Eighth Day of Creation*. (Simon & Schuster, New York, 1979).
15. Ellis, E. L. & Delbruck, M. The growth of bacteriophage. *The Journal of General Physiology* vol. 22 365–384 (1939).
16. Levin, B. R., Stewart, F. M. & Chao, L. Resource-limited growth, competition, and predation: a model and experimental studies with bacteria and bacteriophage. *The American Naturalist* **111**, 3–24 (1977).
17. Weitz, J. S. *Quantitative Viral Ecology: Dynamics of Viruses and Their Microbial Hosts*. (Princeton Press, 2016).
18. Levin, B. R., Stewart, F. M. & Chao, L. Resource-limited growth, competition, and predation: a model and experimental studies with bacteria and bacteriophage. *American Naturalist* **111**, 3–24 (1977).
19. Bohannan, B. J. M. & Lenski, R. E. Effect of resource enrichment on a chemostat community of bacteria and bacteriophage. *Ecology* **78**, 2303–15 (1997).
20. Bohannan, B. J. M. & Lenski, R. E. Linking genetic change to community evolution: insights from studies of bacteria and bacteriophage. *Ecology Letters* **3**, 362–377 (2000).
21. Chao, L., Levin, B. R. & Stewart, F. M. A complex community in a simple habitat: An experimental study with bacteria and phage. *Ecology* vol. 58 369–378 (1977).
22. Buckling, A. & Rainey, P. B. Antagonistic coevolution between a bacterium and a bacteriophage. *Proceedings of the Royal Society of London Series B-Biologial Sciences* **269**, 931–6 (2002).
23. Betts, a., Kaltz, O. & Hochberg, M. E. Contrasted coevolutionary dynamics between a bacterial pathogen and its bacteriophages. *Proceedings of the National Academy of Sciences* **111**, (2014).
24. Weitz, J. S. *et al.* Phage–bacteria infection networks. *Trends in microbiology* **21**, 82–91 (2013).

25. Poisot, T., Lepennetier, G., Martinez, E., Ramsayer, J. & Hochberg, M. E. Resource availability affects the structure of a natural bacteria–bacteriophage community. *Biology letters* **7**, 201–204 (2011).
26. Flores, C. O., Valverde, S. & Weitz, J. S. Multi-scale structure and geographic drivers of cross-infection within marine bacteria and phages. *The ISME journal* **7**, 520–532 (2013).
27. Kauffman, K. M. *et al.* Resolving the structure of phage–bacteria interactions in the context of natural diversity. *Nat Commun* **13**, 372 (2022).
28. Gupta, A. *et al.* Leapfrog dynamics in phage-bacteria coevolution revealed by joint analysis of cross-infection phenotypes and whole genome sequencing. *Ecology letters* **25**, 876–888 (2022).
29. Tropini, C., Earle, K. A., Huang, K. C. & Sonnenburg, J. L. The gut microbiome: Connecting spatial organization to function. *Cell Host Microbe* **21**, 433–442 (2017).
30. Kerr, B., Neuhauser, C., Bohannan, B. J. M. & Dean, A. M. Local migration promotes competitive restraint in a host–pathogen "tragedy of the commons". *Nature* **442**, 75–78 (2006).
31. Kerr, B., Riley, M. A., Feldman, M. W. & Bohannan, B. J. M. Local dispersal promotes biodiversity in a real-life game of rock-paper-scissors. *Nature* **418**, 171–174 (2002).
32. Eriksen, R. S., Mitarai, N. & Sneppen, K. Sustainability of spatially distributed bacteria-phage systems. *Sci Rep* **10**, 3154 (2020).
33. Wei, W. & Krone, S. M. Spatial invasion by a mutant pathogen. *Journal of Theoretical Biology* **236**, 335–348 (2005).
34. Bull, J. J. *et al.* Phage-bacterial dynamics with spatial structure: Self organization around phage sinks can promote increased cell densities. *Antibiotics (Basel)* **7**, (2018).
35. Ashby, B., Gupta, S. & Buckling, A. Spatial Structure Mitigates Fitness Costs in Host-Parasite Coevolution. *The American Naturalist* **183**, E64–E74 (2014).
36. Heilmann, S., Sneppen, K. & Krishna, S. Coexistence of phage and bacteria on the boundary of self-organized refuges. *Proc. Natl. Acad. Sci. U. S. A.* **109**, 12828–12833 (2012).

37. Simmons, E. L. *et al.* Biofilm Structure Promotes Coexistence of Phage-Resistant and Phage-Susceptible Bacteria. *mSystems* **5**, 10.1128/msystems.00877-19 (2020).

38. Janzen, D. H. Herbivores and the Number of Tree Species in Tropical Forests. *American Naturalist* **104**, 501–528 (1970).

39. Connell, J. H. On the role of natural enemies in preventing competitive exclusion in some marine animals and in rain forest trees. in *Dynamics of Populations* (eds. Boer, P. J. D. & Gradwell, G. R.) (Pudoc, Wageningen, 1970).

40. Ping, D. *et al.* Hitchhiking, collapse, and contingency in phage infections of migrating bacterial populations. *ISME J* **14**, 2007–2018 (2020).

41. Shaer Tamar, E. & Kishony, R. Multistep diversification in spatiotemporal bacterial-phage coevolution. *Nat Commun* **13**, 7971 (2022).

42. Li, X., Gonzalez, F., Esteves, N., Scharf, B. E. & Chen, J. Formation of phage lysis patterns and implications on co-propagation of phages and motile host bacteria. *PLOS Computational Biology* **16**, e1007236 (2020).

43. Cremer, J. *et al.* Chemotaxis as a navigation strategy to boost range expansion. *Nature* **575**, 658–663 (2019).

44. Namiko, M., Stanley, B., Kim, S. & J, S. T. Population Dynamics of Phage and Bacteria in Spatially Structured Habitats Using Phage Lambda and Escherichia coli. *Journal of Bacteriology* **198**, 1783–1793 (2021).

45. Weitz, J. S. & Dushoff, J. Alternative stable states in host–phage dynamics. *Theoretical Ecology* **1**, 13–19 (2008).

46. Wang, Z. & Goldenfeld, N. Fixed points and limit cycles in the population dynamics of lysogenic viruses and their hosts. *Phys. Rev. E* **82**, 011918 (2010).

47. Dominguez-Mirazo, M., Harris, J. D., Demory, D. & Weitz, J. S. Accounting for cellular-level variation in lysis: implications for virus–host dynamics. *Mbio* **15**, e01376-24 (2024).

48. Berg, H. C. *Random Walks in Biology*. (Princeton University Press, Princeton, NJ, 1993).

49. Nguyen, T. V. P. *et al.* Coinfecting phages impede each other's entry into the cell. *Current Biology* **34**, 2841-2853.e18 (2024).

50. Narla, A. V., Cremer, J. & Hwa, T. A traveling-wave solution for bacterial chemotaxis with growth. *Proceedings of the National Academy of Sciences* **118**, e2105138118 (2021).

51. Tu, Y., Shimizu, T. S. & Berg, H. C. Modeling the chemotactic response of *Escherichia coli* to time-varying stimuli. *Proceedings of the National Academy of Sciences* **105**, 14855–14860 (2008).

52. van der Kolk, J. *et al.* Anomalous Collective Dynamics of Autochemotactic Populations. *Phys. Rev. Lett.* **131**, 088201 (2023).

53. Kayser, J., Schreck, C. F., Gralka, M., Fusco, D. & Hallatschek, O. Collective motion conceals fitness differences in crowded cellular populations. *Nature Ecology & Evolution* **3**, 125–134 (2019).

54. Nikolic, N., Anagnostidis, V., Tiwari, A., Chait, R. & Gielen, F. Droplet-based methodology for investigating bacterial population dynamics in response to phage exposure. *Frontiers in Microbiology* **14**, 1260196 (2023).

55. Möbius, W., Murray, A. W. & Nelson, D. R. How Obstacles Perturb Population Fronts and Alter Their Genetic Structure. *PLOS Computational Biology* **11**, e1004615 (2015).

56. Yap, M. L. & Rossmann, M. G. Structure and Function of Bacteriophage T4. *Future Microbiology* **9**, 1319–1327 (2014).

57. Grace, A., Sahu, R., Owen, D. R. & Dennis, V. A. Pseudomonas aeruginosa reference strains PAO1 and PA14: A genomic, phenotypic, and therapeutic review. *Front Microbiol* **13**, 1023523 (2022).

58. Krylov, V. *et al.* Phage phiKZ—The First of Giants. *Viruses* **13**, 149 (2021).

59. Kropinski, A. M., Mazzocco, A., Waddell, T. E., Lingohr, E. & Johnson, R. P. Enumeration of Bacteriophages by Double Agar Overlay Plaque Assay. in *Bacteriophages: Methods and Protocols, Volume 1: Isolation, Characterization, and Interactions* (eds. Clokie, M. R. J. & Kropinski, A. M.) 69–76 (Humana Press, Totowa, NJ, 2009). doi:10.1007/978-1-60327-164-6_7.

60. Baym, M. *et al.* Spatiotemporal microbial evolution on antibiotic landscapes. *Science* **353**, 1147–1151 (2016).

61. Stroustrup, N. *et al.* The Caenorhabditis elegans Lifespan Machine. *Nat Meth* **10**, 665–670 (2013).

62. Schindelin, J. *et al.* Fiji: an open-source platform for biological-image analysis. *Nat Methods* **9**, 676–682 (2012).

$$
\begin{aligned}
\frac{\partial R(\mathbf{x},t)}{\partial t} &= -\,g(R)B(\mathbf{x}) + D_R\nabla^2 R(\mathbf{x}),\\
\frac{\partial a_n(\mathbf{x},t)}{\partial t} &= -\,\mu_n(a_n)B(\mathbf{x}) + D_R\nabla^2 a_n(\mathbf{x}),\\
\frac{\partial S(\mathbf{x},t)}{\partial t} &= g(R)S(\mathbf{x}) - S(\mathbf{x})T(P)F(P) + D_B\nabla^2 S(\mathbf{x}) + \sum_n \boldsymbol{\nabla}\cdot\left[S(\mathbf{x})\boldsymbol{v}_n(a_n(\mathbf{x}))\right],\\
\frac{\partial E_1(\mathbf{x},t)}{\partial t} &= S(\mathbf{x})T(P)F(P) - L\eta(R)E_1(\mathbf{x}) + D_B\nabla^2 E_1(\mathbf{x}) + \sum_n \boldsymbol{\nabla}\cdot\left[E_1(\mathbf{x})\boldsymbol{v}_n(a_n(\mathbf{x}))\right],\\
\frac{\partial E_{i\in\{2\ldots L\}}(\mathbf{x},t)}{\partial t} &= L\eta(R)E_{i-1}(\mathbf{x}) - L\eta(R)E_i(\mathbf{x}) + D_B\nabla^2 E_i(\mathbf{x}) + \sum_n \boldsymbol{\nabla}\cdot\left[E_i(\mathbf{x})\boldsymbol{v}_n(a_n(\mathbf{x}))\right],\\
\frac{\partial P(\mathbf{x},t)}{\partial t} &= \beta(R)L\eta(R)E_L(\mathbf{x}) - B(\mathbf{x})T(P)F(P) - \omega PT(P) + D_P\nabla^2 P(\mathbf{x})
\end{aligned}
$$

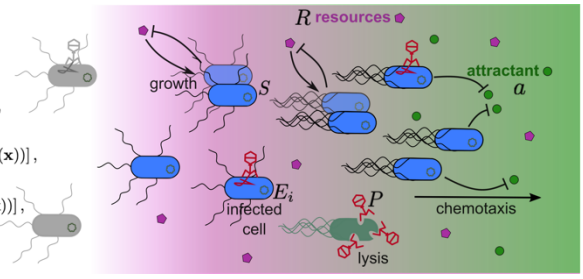


**Box 1 Figure**

**Caption:**
Spatial PDE model governing the spatiotemporal concentrations of chemotaxing susceptible ($S$) and virulent phage-infected ($E_i$) bacteria, phage $P$, resources $R$ (magenta gradient) and chemoattractant $a$ (green gradient). Bacteria feed on resources at a rate $g(R)$, generating a spatial chemical gradient. As a result, bacteria chemotax towards higher attractant concentrations through the self-generated velocity field $v(a)$, triggering a collective range expansion wave. Free phage infect bacteria and infected cells chemotax before lysing. All agents diffuse according to a specific diffusion constant $D$.

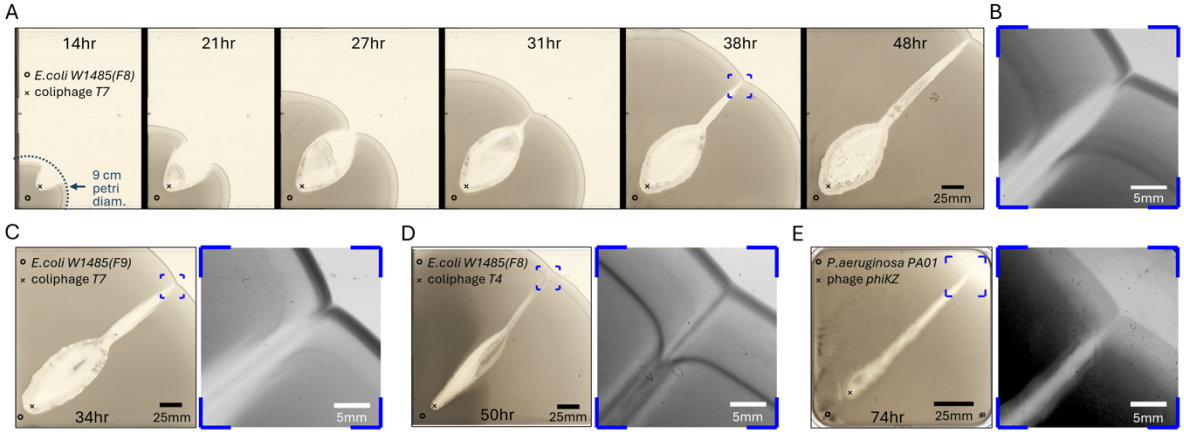


**Figure 1 Extended regions cleared by lytic phage emerge and resolve to stably propagating infections on chemotaxing bacterial fronts.**

**(A)** Time-lapse transmission scans of an expanding *E.coli* W1485(F8) population, chemotaxing through 0.25% agar nutrient media from point "o" near the corner of a 24cm plate. The bacterial front is invaded by virulent T7 phage particles it encounters at point "x". While still diverging at the scale of a center-inoculated 9cm swim assay plate after 14hr, the phage-cleared region reconverges by 30hr and settles into a narrow stable propagation across the rest of the test plate. Scale bar 25mm **(B)** A zoomed, linearly contrast-enhanced view of the stably propagating infection front in panel A at 38hr (blue box). Similar virulent phage invasions, followed by expansion, reconvergence and stable extension of infections with migrating host fronts is seen for **(C)** W1485(F9), an *E.coli* W1485(F8) mutant with a single dominant front, encountering phage T7, **(D)** *E.coli* W1485(F8) encountering phage T4, and **(E)** *P.aeruginosa* PA01 encountering phage ΦKZ. Transmission scans (left) and linearly contrast-enhanced zooms (right) are shown for indicated 25mm regions (blue boxes).

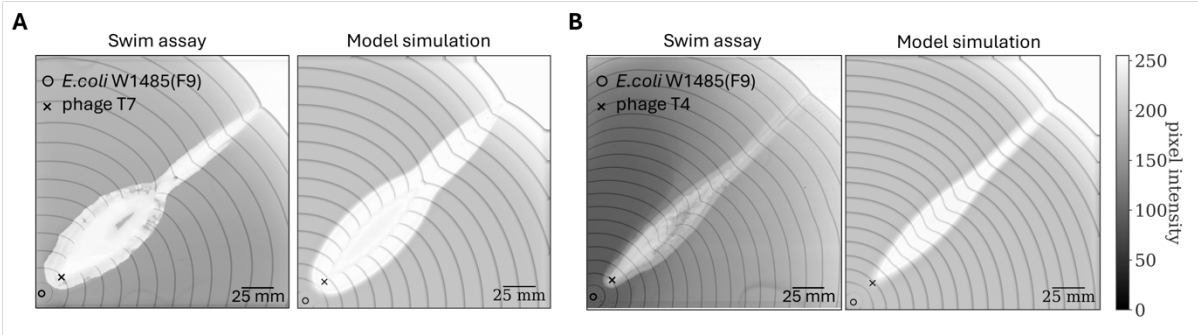


**Figure 2: Phage Amplified Spatially Extended Regions observed in experiments and model simulation**
Images of populations (grey) of *E.coli* strain W1485(F9) growing and chemotaxing from location ○**,** that encountered **(A)** T7 or **(B)** T4 phages at location × in 24x24cm soft agar swim assays. In both cases, elongated, clear invasion transients appear and resolve to narrow, stably propagating infections. Experimental data (blue channel of color transmission scans) are displayed to the left and model simulations (cell densities mapped to calibrated blue channel pixel intensities, Methods) shown to the right. The positions of the dominant chemotactic front (grey curves) of W1485(F9) are overlaid on each image at 2 hour intervals to highlight its shape and trajectory throughout the infection without confounding by continued phage lysis behind the migrating fronts. See also Supplementary Movies 2-5. All simulation parameters are indicated in Supplementary Text Table S1, except for A) where we modulate the bacteria diffusion constant $D_B = 2.7 \cdot 10^5 \mu m^2$/hrs and responsiveness to sensed gradient $\chi = 5.5 \cdot 10^6 \mu m^2$/hrs to match the faster range expansion (around 7.2 mm/hr) in this experimental replicate.

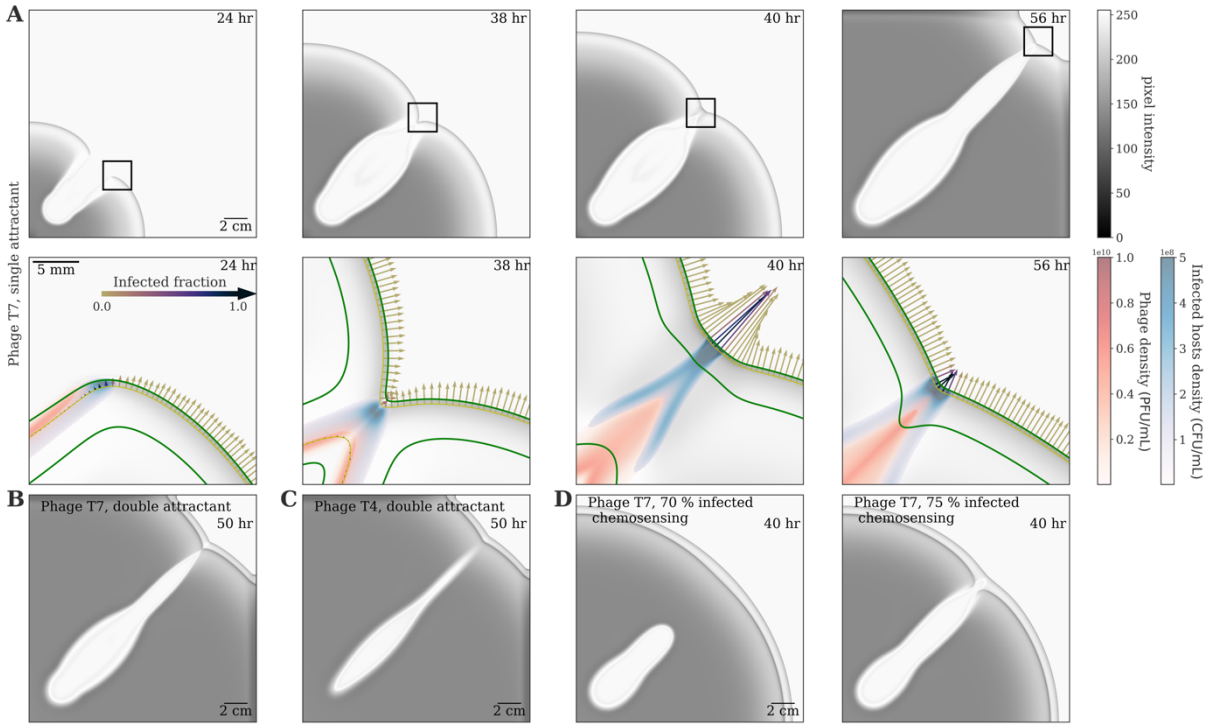


**Figure 3. Model of phage infections transport by chemotactically migrating bacteria populations**.

**(A)** Timepoints of a simulation using the model defined in Box 1, with parameters inferred for *E. coli* W1485(F8) and phage T7 (see Supplementary Text) and a single attractant (yielding a single chemotactically migrating front). Pixel intensity is mapped from calibrated cell density (Methods). The macroscale spatiotemporal dynamics (top) closely resemble the patterns of Fig.1A. Bottom: insets showing density of total (grey) and infected (blue) cells and density of phages (red). The two green lines represent attractant density isolines at half the initial value and at the lower sensing threshold. The thin yellow line, close to the front, denotes the isoline where the chemosensing response is at 80% its maximum. Quivers represent the chemotactic flux along this line, colored according to the fraction of infected cells. **(B)** Snapshot of the same simulation as **A**, with the addition of a second attractant. The qualitative behavior (invasion transient and coalescence to a stably propagating infection) of the model is not affected by the resulting dual migration fronts. **(C)** Simulations with viral life-traits inferred for phage T4, while maintaining all bacterial traits unaltered (see Supplementary Text). The model behaviour transitions to a macroscale pattern closer to the empirical T4 PhASER shown in Figure 1D. **(D)** Accounting for phage-inhibited chemotaxis of infected cells. Model simulations are shown for W1485(F8) encountering phage T7, while modulating infected cell responsiveness to attractant concentrations. The stable infection transport phenomenon persists for a 25% reduction in chemotactic responsiveness of infected cells, but is finally lost as responsiveness is lowered to 70% that of uninfected cells.

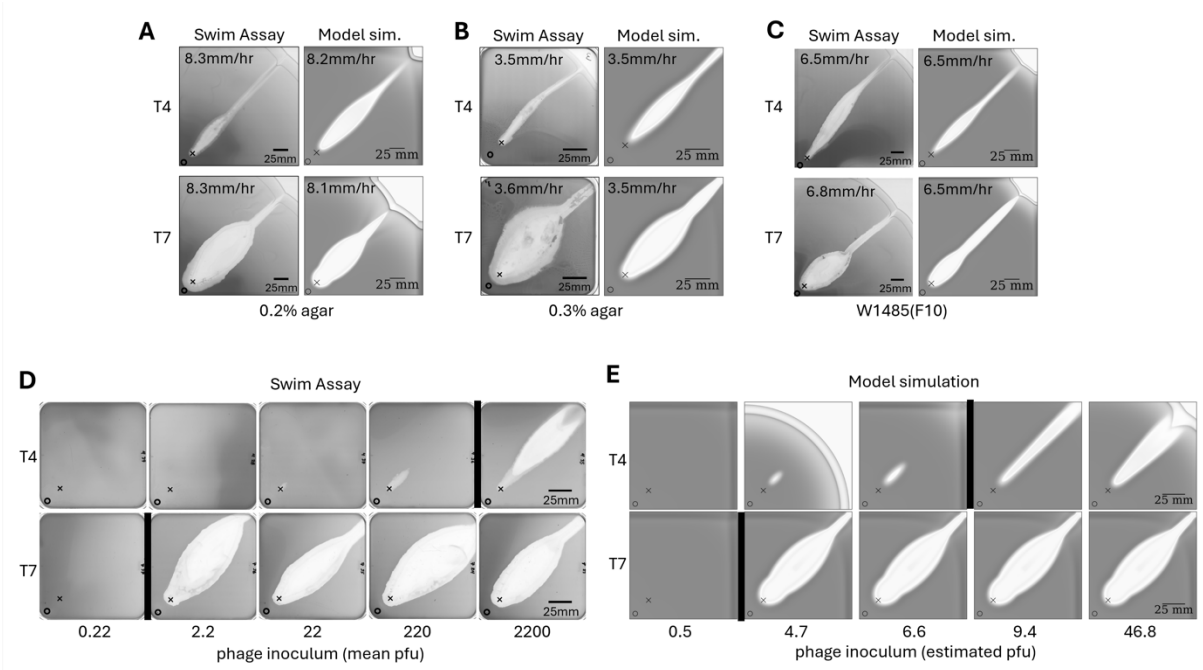


**Figure 4. Stable phage infection transport by chemotaxing bacterial populations is robust to environmental and host changes that impact migration speed, and in phage-dependent manner, to invading phage population size.**

**(A)** Reducing agar concentration in swim assays from 0.25% (Fig 1A) to 0.2% increases *E.coli* W1485(F8) migration rate by ~50%. However, invasions of hosts migrating from location ○ by phages T4 (top) and T7 (bottom) inoculated at location × on 24x24cm assays continue to resolve to stably propagating infections, Experimental data (blue channel of transmission scans) to the left are closely mirrored on the right by model simulations (cell concentration-calibrated blue pixel values) in which host parameters $\chi$ and $D_B$are adjusted to match the front expansion speed (see Supplementary Text Section 2) while T7 and T4 phage parameters are unchanged, showing that the model ingredients encode the observed empirical robustness. **(B)** Similarly, increasing agar concentration to 0.3% slows host migration by approximately 50%. Yet, phages T4 and T7 invade and produce stable PhASERs on 12x12cm plates, indicating that localized phage invasion and stable infection transport in migrating bacterial fronts is robust across a range of environmental perturbations to migration speed. **(C)** T4 and T7 PhASERs robustly emerge on *E.coli* W1485(F10), a spontaneously evolved fast migration mutant of W1485(F8) that maintains two chemotactic fronts (left). Model simulations (right) where the bacterial parameters are quantitatively fit to the new strain (see Supplementary Text Table S1) reproduce the experimental behaviour. **(D)** Effect of the initial phage concentration on PhASER formation is measured by challenging E.coli W1485(F8) migrating from location ○ with few to thousands of plaque forming units (pfu). T4 requires needs ~1000 phage particles to invade and initiate infection transport, while just a few phage T7 particles reliably initiate stable PhASERs (cutoffs indicated by black verticals). **(E)** The qualitative scenario of phage infective dose dependence is reproduced by a modified model, although the quantitative transition from T4 loss to stable infection propagation is steeper than observed in experiment. Critically, the phage inoculum dependence was not reproduced by our original model. Reproducing the qualitative experimental observation required a reduced chemosensing responsiveness of 87% for infected cells, reflecting partial suppression of host chemotactic motility by phage infection.

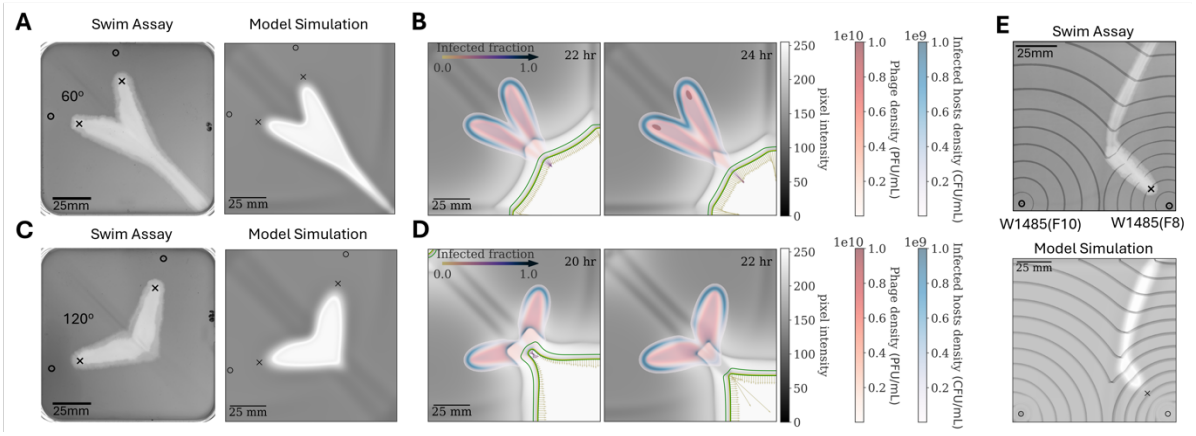


**Fig 5. Geometric dependence of merging and termination of PhASERs on colliding chemotactic waves**

**(A)** Experimental image (left) shows two T4 PhASERs on nearby *E.coli* W1485(F8) colonies that migrated from location ○ and intersected at a 60 degrees angle. The PhASERs merged along the symmetry line (the plate's diagonal) and continued stable progression across the agar plate. This phenomenon is reproduced by the model (right). The parameters correspond to those inferred for *E.coli* W1485(F8) and phage T4. **(B)** Detailed simulation output (see Fig. 2A bottom) at two timepoints shows PhASER merging is driven by increased flux of infected cells along the symmetry line, mediated by attractant profiles, similar to phage T7 stabilization in Figure 2A (Supplementary Movie 6). **(C)** Increasing the intersection angle to 120 degrees halts PhASER infection transport the two colonies collide, both experiments (left) and simulations (right). **(D)** Detailed simulation timepoints show that when the angle between the fronts is too steep, the two colliding fronts merge at a point beyond the phage infections, which are lost behind the front as attractant and nutrients are depleted (Supplementary Movie 7). **(E)** Experiments (top) and simulations (bottom) where a T4 PhASER on *E.coli* W1485(F8) collides with migrating front of a much faster *E.coli* strain W1485(F10), turns sharply and continues in the faster curving interface between the strains (See also Supplementary Movies 8,9). The PhASER transport phenomenon is sufficiently robust that the infection transport dynamically adapts to higher speeds, for instance encountered upon the emergence of a faster mutant, and this robustness is reflected in the model. The simulation parameters are those inferred for phage T4 against W1485(F8) and W1485(F10) respectively (see Supplementary Text Table S1). Time frames are overlaid with 2 hour-spaced front positions (grey curves).

## Methods

Strains

| | Strain | Source | Description |
|---|---|---|---|
| *Escherichia coli* | W1485 | Gift from N.Nikolic[54] | K-12 derivative F+ λ- |
| *Escherichia coli* | W1485(F8) | This work | Rapid migration derivative of W1485. |
| *Escherichia coli* | W1485(F9) | This work | Rapid migration derivative of W1485(F8). Single dominant chemotactic front. |
| *Escherichia coli* | W1485(F10) | This work | Rapid migration derivative of W1485(F8). Maintains two dominant chemotactic fronts. |
| *Escherichia* phage | T7 | Gift from W. Moebius. | Lytic phage of *E.coli* W1485[55] |
| *Escherichia* phage | T4 | Gift from from C.Fitch, B.Temperton | Lytic phage of *E.coli* W1485[56] |
| *P.aeruginosa* | PA01 | Gift from S.Porter. | *P. aeruginosa* reference strain[57] |
| *Pseudomonas* phage | PhiKZ | Gift from S.van Houte. | Lytic phage of *P. aeruginosa* PA01[58] |

Bacterial and phage stocks

All bacterial strains were grown overnight from single colonies to saturation, mixed with glycerol to a final concentration of 17% and stored at as a master stock and single-use aliquots (at concentrations of approximately $10^9$ cfu/ml) -80ºC. Single-use aliquots were thawed for inoculation of liquid cultures or direct inoculation of soft agar swim assays. Viable cell concentrations in stocks were determined by colony counts of thawed, serially-diluted samples.

Phage were amplified by adding cores picked from single plaques on double layer plates to growing host cultures (at $10^7$-$10^8$ cfu/ml). After several hours, clear lysates were centrifuged to remove cell debris and the supernatant was passed through a 0.2µm syringe filter and stored in amber glass vials at 4C. *E.coli* phages were amplified on *E.coli* strain W1485. Phage PhiKZ was grown on *P. aeruginosa* PA01. Plaque forming unit concentrations were determined by serial dilution and plaque counts on double overlay plates[59].

Host migration training for *E.coli*

Soft agar swim assays select for faster migration at the chemotactic front. As faster migrating mutants of *E.coli* W1485 emerge regularly enough to disrupt our swim assays, we passaged this strain across a series of swim assays to obtain more stable, faster migrating derivatives for our experiments[60]. For each passage, we inoculated the most recent isolate at a corner of the plate and transferred the first arrivals at the opposite corner to the next plate. The faster, more stably migrating W1485(F8) was obtained after eight passages. W1485(F9) with a single dominant chemotactic front, and W1485(F10), retaining two fronts, emerged on a ninth passage, and migrated at a similar rate to each other. *P. aeruginosa* PA01 did not show rapid accumulation of fast migration mutants and was not passaged.

Scanner timelapse platform

Two scanner platforms, based on a previously reported design[61] were used to record time-lapse image sequences of swim assays. Each platform includes three Epson V800/850 scanners, that can collect large format (8”x10”) transmission scans. The scanners are connected to a Raspberry Pi 4 computer (Supplementary Figure 8) and controlled by a custom python script (Supplementary Method 1) that

uses Scanner Access Now Easy (http://www.sane-project.org/) and a Sane python interface (https://pypi.org/project/python-sane/) to collect images from all running scanners at user-determined intervals and resolutions. Custom inserts (Supplementary Method 2) are used to align assay plates in the transmission imaging region of the scanner platens.

Swim assays

All swim assays were performed in 12cm (Greiner, 688161) or 24cm (Corning CLS431301) square petri dishes. Low concentration swim agar media was prepared by combining warmed LB (10 g/L tryptone, 5g/L yeast extract, 5g/L NaCl) liquid broth with premelted LB containing 2% Bacto Agar (Difco) in appropriate proportions at 50ºC. Volumes (50ml or 200ml) of mixed media were added to 12cm or 24cm plates, respectively, and allowed to set. Host and phage stocks were inoculated by pipetting (typically) 1µl of each directly into the agar at predefined locations indicated on a map beneath the plate. Plates were then left for 1 hour to absorb the inocula and overlaid with clear mineral oil (Merck, 330779) to prevent evaporation and condensation on lids. Once overlaid, the plate lids were dried of condensation and plates incubated (positioned on transmission scanners if timelapses were to be recorded). Typical timelapses recorded 300dpi colour images at 10 minute intervals.

Image pixel intensity to CFU/ml calibration

We obtained an empirical calibration curve to allow inference of cell concentrations in the swim agar from pixel intensities in our scanned images. To do so, we performed 2-fold serial-dilutions from an overnight (37ºC, 230RPM) culture of *E.coli* W1485. We added 50ml of each dilution to 12x12cm swim assay plates (to match light path length in swim assays). The plates were immediately scanned and fit obtained for media blank-subtracted average pixel levels (blue channel) as a function of corresponding cell concentrations determined by colony forming unit counts. See (Supplementary Figure 9).

Image analysis

Primary image analysis of timelapse images was performed using FIJI software[62]. The blue channel of the colour scan was analyzed as it showed a slightly higher dynamic range in detecting cell density than the red and green channels. Time differential image sequences, extracted from the timelapse image stacks by subtracting each image from the one preceding it, were used to identify cell growth regions and particularly to highlight rapid density changes at migration and lysis fronts (Supplementary Movie 10). Time differentials were binarized to extract migration fronts. Binarized images were denoised with median and morphological close/open filters. Maximum projection of binarized front images through time was used to generate overlays of time-spaced front shapes throughout PhASER swim assays. (Supplementary Figure 3). Front migration rates are determined by displacement of advancing chemotactic fronts in kymographs (obtained using the FIJI multi-kymograph plugin) and conversion to mm/hr units (Supplementary Figure 10).